8-2023

Development and application of a microfluidic platform for quantifying intra-tumoral compressive stress.

Zachary P. Fowler
University of Louisville

DEVELOPMENT AND APPLICATION OF A MICROFLUIDIC PLATFORM FOR QUANTIFYING INTRA-TUMORAL COMPRESSIVE STRESS

By

Zachary P. Fowler

B.S. Bioengineering, University of Louisville, August 2022

A Thesis

Submitted to the Faculty of the

University of Louisville

J.B. Speed School of Engineering

As Partial Fulfillment of the Requirements

for the Professional Degree

MASTER OF ENGINEERING

Department of Bioengineering

August 2023

DEVELOPMENT AND APPLICATION OF A MICROFLUIDIC PLATFORM FOR QUANTIFYING INTRA-TUMORAL COMPRESSIVE STRESS

Submitted by:

Zachary P Fowler

A Thesis Approved on:

August 4, 2023

By the following Reading and Examination Committee:

Joseph Chen Digitally signed by Joseph Chen Date: 2023.08.04 09:20:02 -04'00'

Thesis Chair

Jonathan Kopechek Digitally signed by Jonathan Kopechek Date: 2023.08.04 19:16:23 -04'00'

Committee Member

Cindy Harnett Digitally signed by Cindy Harnett Date: 2023.08.09 13:53:04 -04'00'

Committee Member

Committee Member

Committee Member

ACKNOWLEDGEMENTS

To my friends and family, thank you for the unwavering love and support throughout my extended and unorthodox educational journey. You all are the reason I'm able to remain motivated through the trials and tribulations of academic research. Dr. Joseph Chen, thank you for taking a chance on an inexperienced undergraduate and for helping me develop work ethic, time management, and creativity. Thank you for encouraging scientific curiosity and for leaning into new ideas with enthusiasm. I'm excited to see what the next chapter looks like for us. Dr. Jonathan Kopechek, thank you for being my first true mentor and for extending a seemingly infinite amount of patience and grace. Dr. Cindy Harnett, thank you for your generosity and willingness to share your expertise. This project quite literally would not have succeeded without your support. Landon Teer, Bradley Mahaffey, McKenzie Johnson, and Eric Dong, thank you for accepting me and for the relationships we've formed. I absolutely owe a great deal of this project's success to your all's dedication to the lab and to one other.

ABSTRACT

Cancer progression is linked to the emergence of aberrant mechanical signaling in the tumor microenvironment. Modulation of extrinsic signals, such as ECM stiffness and composition, have been thoroughly explored. However, the development of solid stresses *within* the tumor remains poorly understood. To address this, we have developed a microfluidic platform that generates deformable alginate microbeads that allow for the quantification of compressive stresses generated within a growing glioblastoma (GBM) tumorsphere. PDMS microfluidic devices were fabricated via SU-8 mold with channels ranging from 10μm-40μm in diameter. Fluorescently labeled sodium alginate underwent a cross-linking reaction within the device to generate monodisperse beads proportional to the channel size. Physical characterization of microbeads included ImageJ particle analysis to calculate average diameter and atomic force microscopy to calculate elastic modulus. Microbeads were subsequently embedded into GBM spheroids, and their deformation was tracked longitudinally. Compressive stress distributions were extracted via 2D axisymmetric finite element-based models.

TABLE OF CONTENTS

LIST OF FIGURES

I. INTRODUCTION

Objective

The objective of this thesis is to develop a microfluidic platform used to generate deformable, monodisperse alginate microbeads, followed by embedment into burgeoning GBM tumorspheres and subsequent quantification of the intra-tumoral compressive stresses generated during tumor development.

Glioblastoma

Glioblastoma (GBM) is a highly invasive and aggressive brain cancer, carrying a median survival between 10-14 months and a three-year survival rate of less than 5% [1], [2]. GBM is also the most common form of glioma, a larger family of tumors that arise in the central nervous system (CNS), and accounts for approximately 82% of all cases of malignant gliomas [3]. These poor prognoses are due, in part, to GBM's resistance to standard therapeutic intervention. As glioblastoma develops, two discrete regions within a given tumor emerge – a dense, proliferative core and a motile, invasive rim. This intratumor heterogeneity is thought to confer the recalcitrant behavior observed throughout disease progression [4], [5]. Previous work in our lab used atomic force microscopy (AFM) to analyze 7 patient-matched GBM core and rim samples. The results reveal that core tissue of each tumor was uniformly stiffer than its corresponding rim tissue.

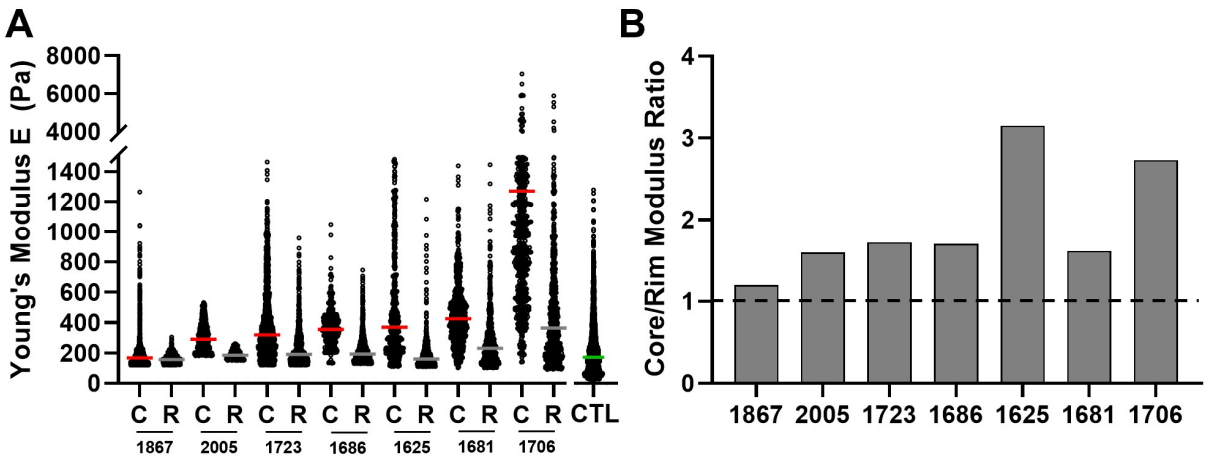

Figure 1: AFM reveals spatial heterogeneity and stiffer core tissue. GBM tumors exhibit heterogeneity in mechanical signatures with tumor core exhibiting higher stiffness when compared to tumor rim and to non-neoplastic controls (A). However, the relative differences between tumor core and rim are patient specific (B).

After describing the mechanical differences between GBM core and rim tissues, SEM was used to investigate the ultrastructural abnormalities and we observed a similar trend/ The core tissue was generally more densely packed and less porous than its corresponding rim tissue. Further, rim tissue contained a greater pore density, which allows for enhanced cell motility and therefore increased invasive potential. This finding is consistent with existing literature and supports hypothesis that GBM cells at the core exhibit more proliferative phenotypes and cells at the rim exhibit more invasive phenotypes. Biophysical signaling from the tumor microenvironment (TME) is considered a driver of these phenotypic changes.

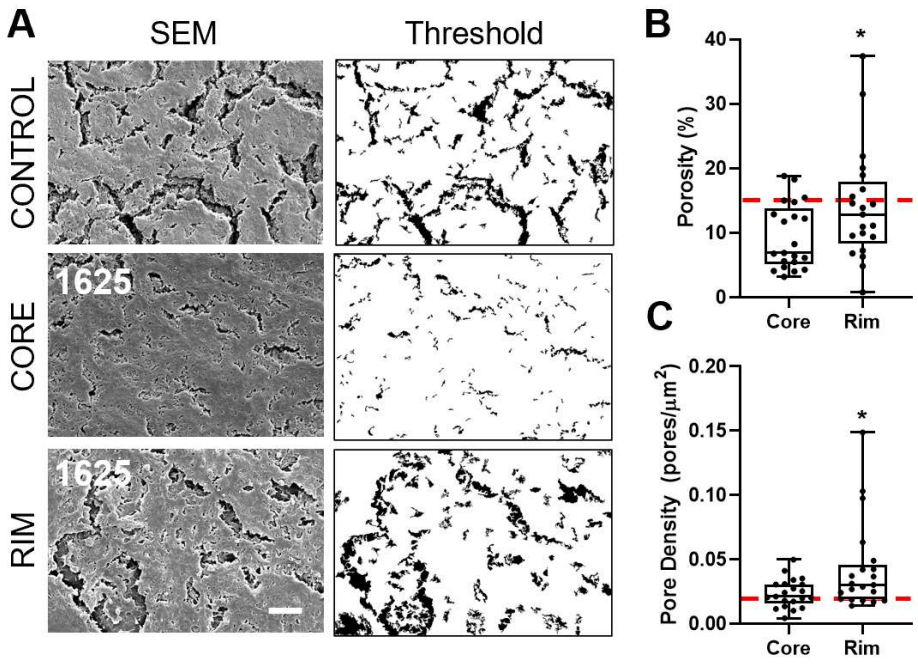

*Figure 2: GBM core displays dense ultrastructure with decreased porosity and pore density. SEM analysis reveals decreased porosity within tumor cores when compared to tumor rim and control samples (A,B). Pore density, the number of pores per area, was also lower in tumor core (C); * - $p < 0.05$, scalebar = 10 μm.*

The Tumor Microenvironment

Features of the brain tumor microenvironment (TME) include the blood-brain barrier, extracellular matrix (ECM), axon-dendrite tracts, and the surrounding glial cells. Under healthy conditions, these systems work in unison to facilitate and modulate neuronal function. However, under aberrant conditions, the signaling cascades derived from these systems contribute to disease progression [6].

Wolf, et al., describe the TME as a dynamic array of signals that drive proliferation, cellular invasion, and resistance to therapeutic intervention. These signals are broadly categorized into chemical, mechanical, topographical, and cellular [7].

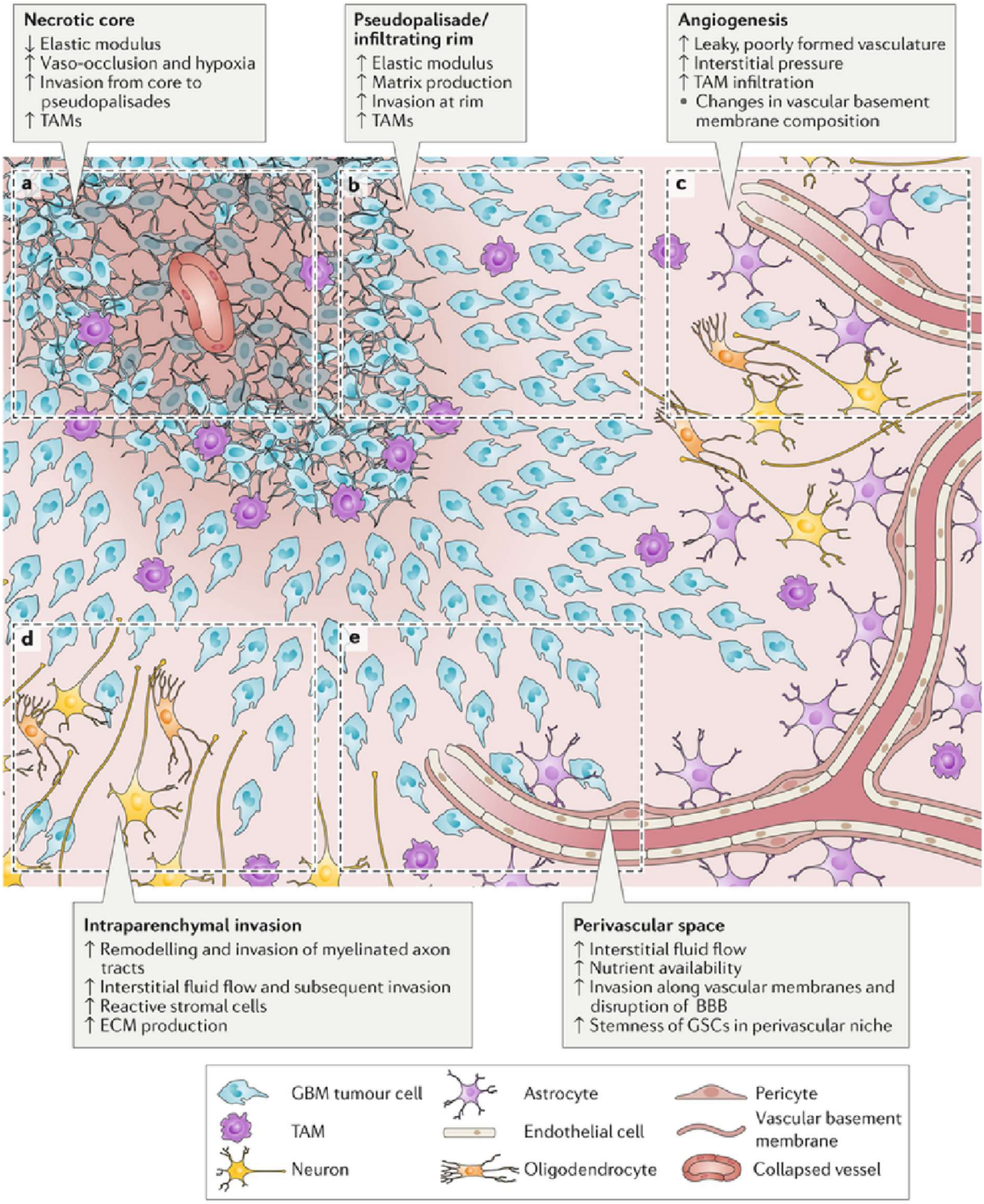

Figure 3: Comprehensive overview of the tumor microenvironment (Wolf, et al., 2019).

For the purposes of our investigation, we will be highlighting ECM mechanical signaling. As the elastic modulus of the *matrix* increases, so does the elastic modulus of the bulk cellular arrangements observed in tumor development. As a result, this increase in stiffness promotes migration and cellular invasion of GBM in vitro – effectively modulating the tumor's locomotive capacity. Further, increased matrix density, which strongly correlates with stiffness, stimulates an active reconstruction of the ECM by GBM cells compared to non-tumor cells. In other words, GBM cells secrete matrix proteins at an advanced rate, which results in high matrix density. Work performed by our lab in tandem with the mechanical and ultrastructural characterization of core and rim tissue showed increases in two major ECM proteins – hyaluronic acid (HA) and tenascin-C (TC) – bolstering the ECM reconstruction hypothesis outlined previously.

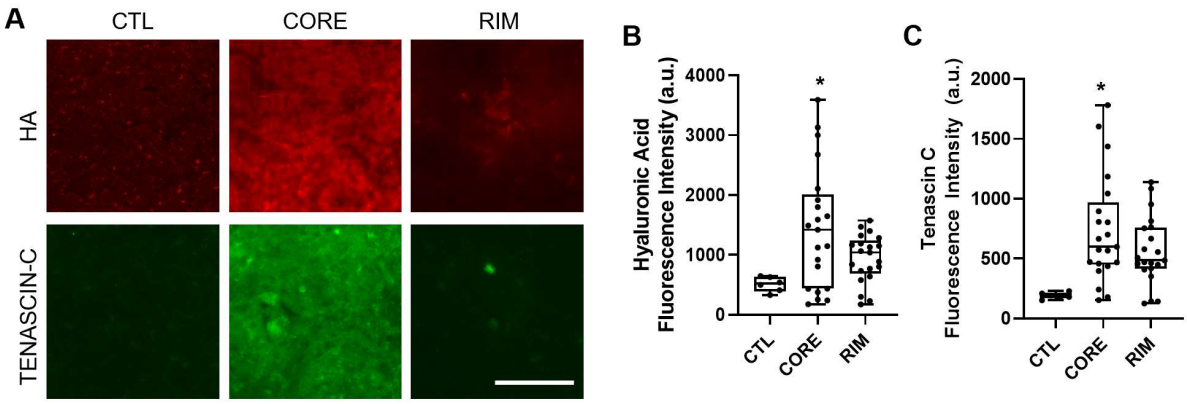

*Figure 4: ECM analysis of tumor core and rim reveal dramatic expression of hyaluronic acid and tenascin-C in tumor cores while tumor rim exhibits non-significant increases compared to control tissue (A-C); * $p < 0.05$, scalebar = 100 μm*

In summary, we have explored the mechanical, ultrastructural, and molecular alterations of the TME associated with tumor evolution and disease progression. The work presented in this thesis aims to quantify the intra-tumoral mechanical response to these biophysical changes.

Alginate Microbeads – Background and Applications

Alginate is a widely used compound in biomedical research due to its biocompatibility, biodegradability, ease of production, and low cost. Commercially available alginate is typically derived from brown algae, which undergoes a series of reactions and purifications to yield sodium alginate. Free calcium ions, typically provided via aqueous solution of calcium chloride, act as a crosslinker for alginate and facilitate the gelation process. Alginate microbeads can be synthesized using a host of techniques, such as single emulsion, double emulsion, spray drying, and microfluidic methods – the morphological demands of the alginate beads dictate the synthetic route. The most common procedure for generation of alginate microbeads between 10-50µm in diameter is water-in-oil emulsion within the confines of a microfluidic device [8]:

Chen, et al. (2013, Royal Society Publishing) demonstrated a method for one-step synthesis of alginate microbeads using the microfluidic water-in-oil method described previously.

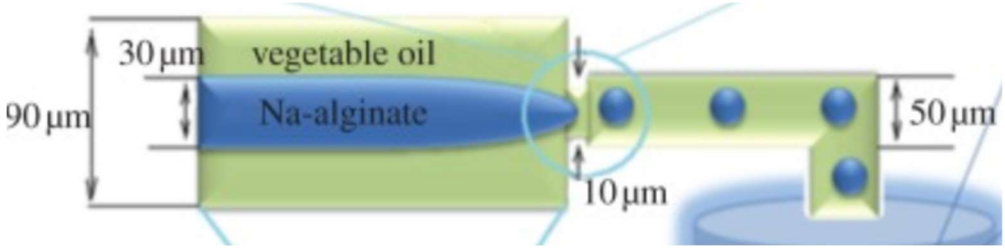

Figure 5: Schematic of the microfluidic generation of monodisperse alginate beads (Chen, et al., 2013)

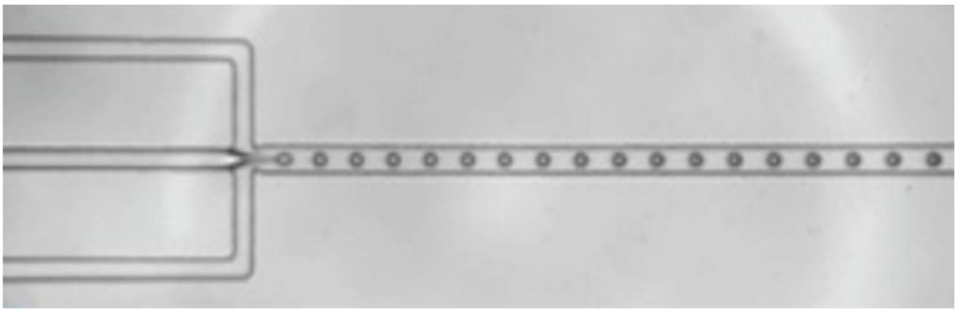

Figure 6: Brightfield (10X) image of droplet generation within a microfluidic device (Chen, et al., 2013)

Here, the dispersed phase (shown in blue in Figure 3 and within the central channel in Figure 4) contains a 1% w/v sodium alginate solution (aq.) and the continuous phase (shown in green in Figure 3 and within the outer channels in Figure 4) contains a 5% w/v Span-80 solution in soybean oil. Span-80 is a hydrophobic surfactant that prevents the aggregation of microbeads after formation. After collection, these microbeads were conjugated with immobilized antibodies and binding affinity for target cells was assessed. Their results demonstrated that these antibodies, incorporated into the nanoporous surface area of the alginate microbeads, maintained binding affinity in a hydrated state [9].

Utech, et al. (2015, Advanced Healthcare Materials) presents a method for microfluidic development of a micron-sized 3D cell culture system which also leverages water-in-oil droplet formation. Additionally, using intra-device ionic crosslinking, they generate monodisperse, structurally homogenous alginate microbeads for single cell encapsulation. They employ two continuous phases – both of which are comprised of perfluoronated carbon oil (PFO). The phase creates the geometric and mechanical conditions for bead formation at a flow-focused junction. The second, containing PFO

with 0.05% v/v acetic acid, induces a reduction in pH that frees calcium ions for crosslinking within the device.

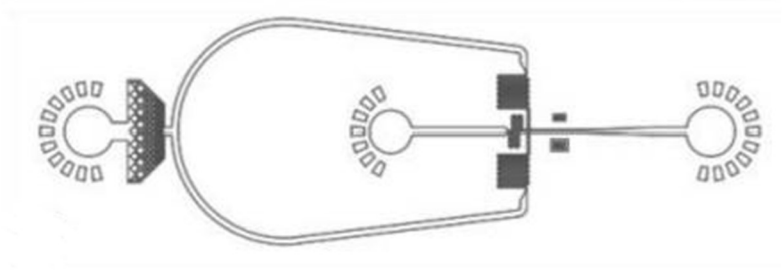

Figure 7: Schematic illustration of microfluidic flow-focusing device. (Utech, et al., 2015)

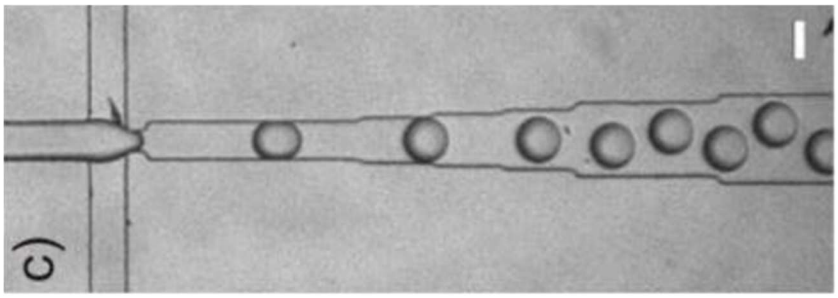

Figure 8: Enhanced view of flow-focused junction for generation of alginate microbeads. Scale bar = 50μm. (Utech, et al., 2015)

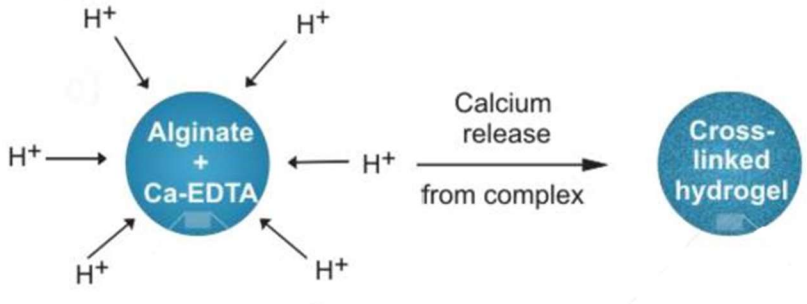

Figure 9: Alginate crosslinking reaction that occurs after pH reduction. When introduced to acidic conditions, the calcium-EDTA complex within the aqueous phase dissolves, releasing free calcium ions. (Utech, et al., 2015)

Mesenchymal stem cells (MSCs) were cultured routinely, trypsinized, and resuspended into the alginate-Ca-EDTA solution, which constitutes the dispersed phase. The device was run again, using the cell laden alginate solution, and they found that 25% of droplets formed contained cell and the remaining 75% remained empty. Calcein-AM staining of the cells within the microgels revealed that 83% of the MSCs remained viable after the encapsulation and crosslinking events [10].

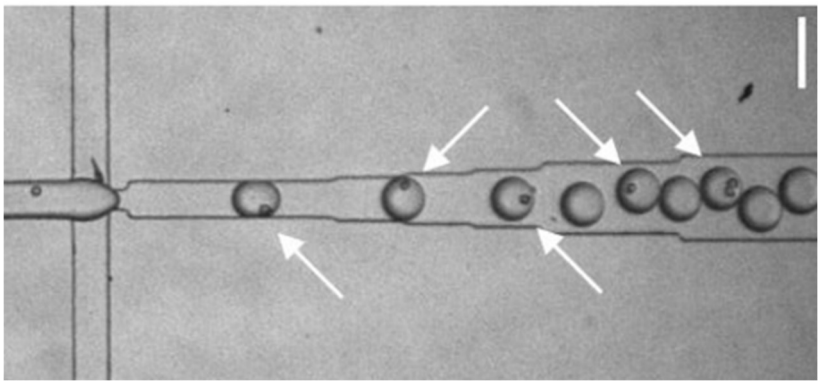

Figure 10: Cells are encapsulated using a 50µm flow focusing device. Single cell containing droplets are indicated by white arrows. Scale bar = 100µm. (Utech, et al., 2015)

While our efforts are directed towards embedding alginate microbeads into tumorspheres rather than encapsulating single cells, this work served as an informative base upon which our flow focused device, bead collection, and cellular incorporation strategies were formed. This thesis aims to integrate the knowledge gained from investigating the tumor microenvironment and microfluidic systems to fill an existing gap in our understanding of disease progression.

II. MATERIALS AND METHODS

Microfluidic Device Design

Microfluidic devices were designed using AutoCAD 2023 and include two semicircular inlets and one circular outlet with diameters of 2.5mm and 4.0mm, respectively. Inlets also contained a tapered design to form the channel entries to encourage flow. The dispersed phase, which contained the sodium alginate solution, flowed through a central horizontal channel with a width of 40µm and a height of 35µm. The continuous phase, which contained a hydrophobic surfactant in soybean oil, flowed through channels with a width of 50µm and a height of 35µm. The "pinch" geometry, ultimately responsible for bead formation and located just beyond the flow-focus junction, had width of 17µm between two arcs with radii of 30µm. It is here that the alginate solution and soybean oil interface. A collection reservoir followed, with a height of either 32 or 50µm depending on the device and a width of approximately 150µm.

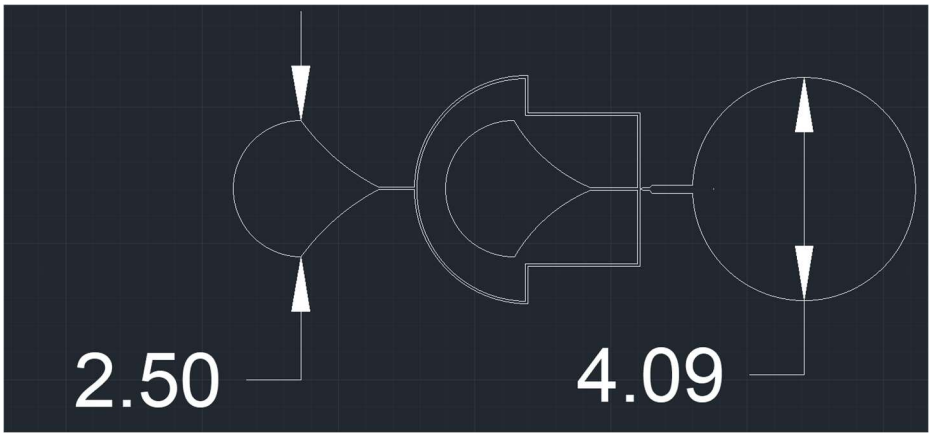

Figure 11: Device design including dimensions of inlets and outlets (mm).

Figure 12: Design and dimensions of flow-focused junction and pinch geometry (mm).

AutoCAD drawing files were saved in .dxf format and forwarded to the Micro/Nano Technology Center (MNTC) in Shumaker Research Building for fabrication of an SU-8 mold using the following procedure [11]:

A. Dehydration

1. Set the temperatures for three hotplates to 65°C, 95°C, and 115°C.

2. Remove the desired photoresist from the refrigerator and let it warm up to room temperature before opening.

3. Take a bare Silicon wafer and clean it. Leave it on the 115°C hotplate for 3 minutes to ensure the wafer is dehydrated before spinning resist. If adhesion is a problem, higher temperatures here (around 150°C) can yield better results.

4. Make sure the wafer is cooled and the Photoresist is at room temperature before spinning.

B. Spinning

1. Adjust the settings on the spinner bench to: SPREAD: Ramp - 100 RPM/sec, Speed - 500 RPM, 0 sec SPIN: Ramp - 500 RPM/sec, Speed - 3000 RPM, 30 sec

2. Dispense about a 4 cm diameter blob of your chosen SU8 onto the center of your Silicon wafer (rotate the wafer to ensure the blob is centered).

3. Center the wafer on the spinner chuck and run the spinner.

C. Soft Bake

1. Remove the wafer from the spinner and use acetone if necessary to remove any SU8 from the bottom of the wafer

2. Place the wafer on the 65°C hotplate for 5 minutes.

3. Transfer the wafer to the 95°C hotplate for 5 minutes.

4. Bake time can depend on the age of the SU8 among other variables, so to ensure that baking is finished take the wafer off the hotplate for a minute and tap the corner of the wafer with tweezers. If the SU8 is still sticky, it needs further baking so briefly return to the 65°C and transfer to the 95°C hotplate again.

D. Exposure

1. Expose the photoresist to 150-160 mJ/cm^2 for 60 seconds.

E. Post-Exposure Bake

1. For SU8, a post exposure bake is necessary for development to function properly.

2. Place the wafer on the 65°C hotplate for 6 minutes.

3. Transfer the wafer to the 95°C hotplate for 6 minutes.

4. The image of the exposure should be clearly visible in the photoresist at this time.

F. Development

1. Fill up an appropriately sized pan with enough PGMEA (aka BTS 220) to keep the wafer submerged.

2. Follow the chart below for an estimate of appropriate development times, agitating sparingly.

3. When done with development rinse the wafer with Isopropanol or the squeeze bottle of SU8 developer

4. Thoroughly dry the wafer before proceeding to hard bake.

G. Hard Bake

1. Place the wafer on the 115°C hotplate for 5 minutes at minimum, longer for thicker resists. If thermal processing with mold is anticipated, make sure to hard bake at least 10°C higher than the anticipated processing temperature.

2. The Hard Bake process is designed to strengthen features and remove cracks that may have formed on the surface of the SU8.

Figure 13: SU-8 mold containing microfluidic devices designed on AutoCAD.

The SU-8 mold was subsequently received from the MNTC cleanroom and transported to the laboratory. Sylgard 184 Elastomer and corresponding curing agent were mixed in a 10:1 ratio (total 50g) and poured directly onto the SU-8 mold. This complex was placed under vacuum and degassed for at least two hours, or until gas bubbles are no longer present. Next, the elastomer and mold were baked overnight at 65°C. After baking, a surgical feather blade was used to cut the individual devices out of the mold and placed device-side-down onto Scotch tape. 1.25 and 3.0mm biopsy punches were used to create the inlets and outlet, respectively. Individually punched devices were

then plasma treated (Harrick), covalently bound to uncharged glass microscope slides, and baked at 65℃ for 48 hours.

Figure 14: Degassing PDMS after pouring onto clean SU-8 mold.

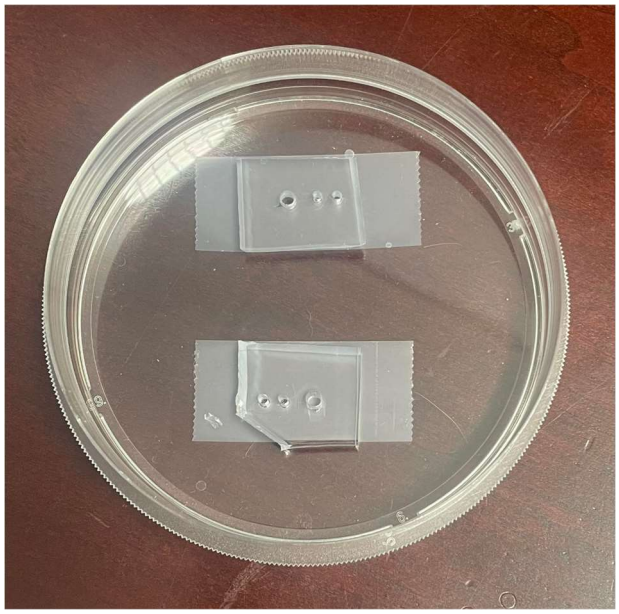

Figure 15: Individual PDMS devices cut and removed from SU-8 mold. 1.25mm diameter holes represent the inlets, and 3.0mm hole represents the outlet.

III. RESULTS AND DISCUSSION

Alginate Microbeads – Synthesis and Characterization

As stated, the microfluidic device contains two phases – a dispersed phase and a continuous phase. The dispersed phase is a 1% w/v sodium alginate solution (aq.) and the continuous phase is soybean oil containing 1% w/v Span-80 (polysorbate 80), which is a hydrophobic, biodegradable surfactant used to prevent alginate aggregation after bead formation. The two solutions are introduced to their respective inlets and each paired with a syringe pump for modulation of flow rate. The dispersed phase maintains a constant flow rate of 50μL/hr, while the continuous phase flow rate may be tuned between 150-550μL/hr. It should be noted that droplet generation requires real-time observation of the solutions' interactions, particularly at the flow-focused junction, so the microfluidic device was mounted onto a microscope stage and flow dynamics observed through 20X magnification. Microbead formation is well described in existing literature and may be determined by the following equations [12]:

$$\frac{L}{w} = 1 + \alpha\left(\frac{Q_{disp.}}{Q_{cont.}}\right) \tag{1}$$

where: L = droplet length

w = channel width

α = geometric constant (~1)

Q_{disp} = dispersed phase flow rate

Q_{cont} = continuous phase flow rate

Q_{disp} will remain constant at 50µL/hr, channel width is a constant 50µm, and Q_{cont} will be adjusted in real-time as flow is observed. In order to achieve spherical droplet formation, the ratio of droplet length to channel width should be approximately 1. Thus, the continuous phase flow rate must be significantly greater than the dispersed phase flow rate to minimize the $\frac{Q_{disp.}}{Q_{cont.}}$ term.

These flow rates determine *capillary number* (C_a), which is the ratio of viscous forces to interfacial forces in the dynamics of capillary flow. Capillary number is a dimensionless group that is often used to analyze fluid flow characteristics, and is described by the following equation [13]:

$$C_a = \left(\frac{\mu_c * v}{\gamma}\right) \tag{2}$$

where: C_a = capillary number
μ_c = continuous phase viscosity
v = dispersed phase velocity
γ = interfacial tension between the dispersed and continuous phases

Capillary number therefore determines droplet length (L) of the dispersed phase based on the interfacial and viscous forces, such that:

Ca < 0.01 results in long droplet formation and L >> w
Ca > 1 results in colinear flow of solutions and L = ∞
0.01 < C_a < 1 encourages spherical droplet formation and L ≅ w

The following values were selected for the dispersed and continuous flow rates:

Q_{disp} = 50µL/hr

Q_{cont} = 450µL/hr

Which resulted in the following calculations:

$$\frac{L}{w} = 1 + \alpha\left(\frac{Q_{disp.}}{Q_{cont.}}\right) = 1 + (1)\left(\frac{\frac{50\mu l}{hr}}{\frac{450\mu L}{hr}}\right) = 1.11$$

$$C_a = \left(\frac{\mu_c * v}{\gamma}\right) = \left(\frac{50cP * (.028m/s)}{\left(\frac{26.25mN}{m}\right)}\right) = 0.0533$$

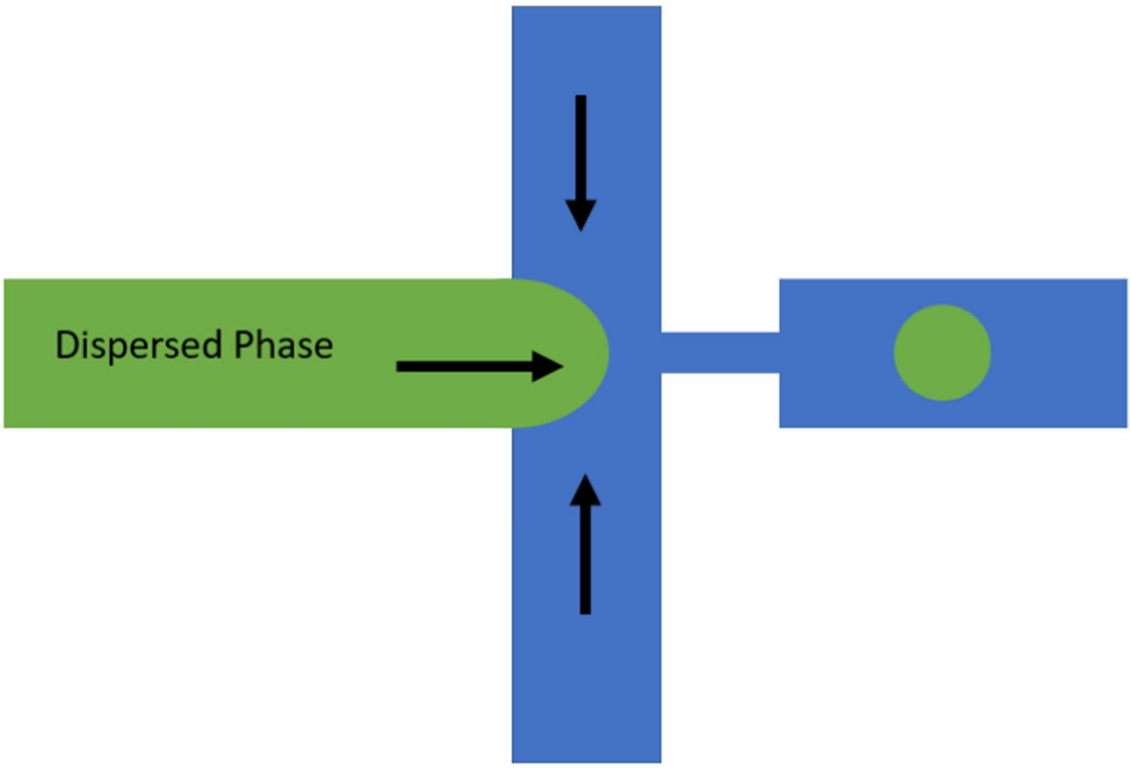

Figure 16: Schematic of flow-focused junction resulting in alginate microbead formation. Dispersed represented in green and continuous phase in blue.

Using the parameters and values described above, we were able to generate monodisperse, spherical alginate hydrogels. Beads were collected from the outlet and placed in 1% $CaCl_2$ solution to initiate cross-linking. The following series of images was taken during real-time bead formation.

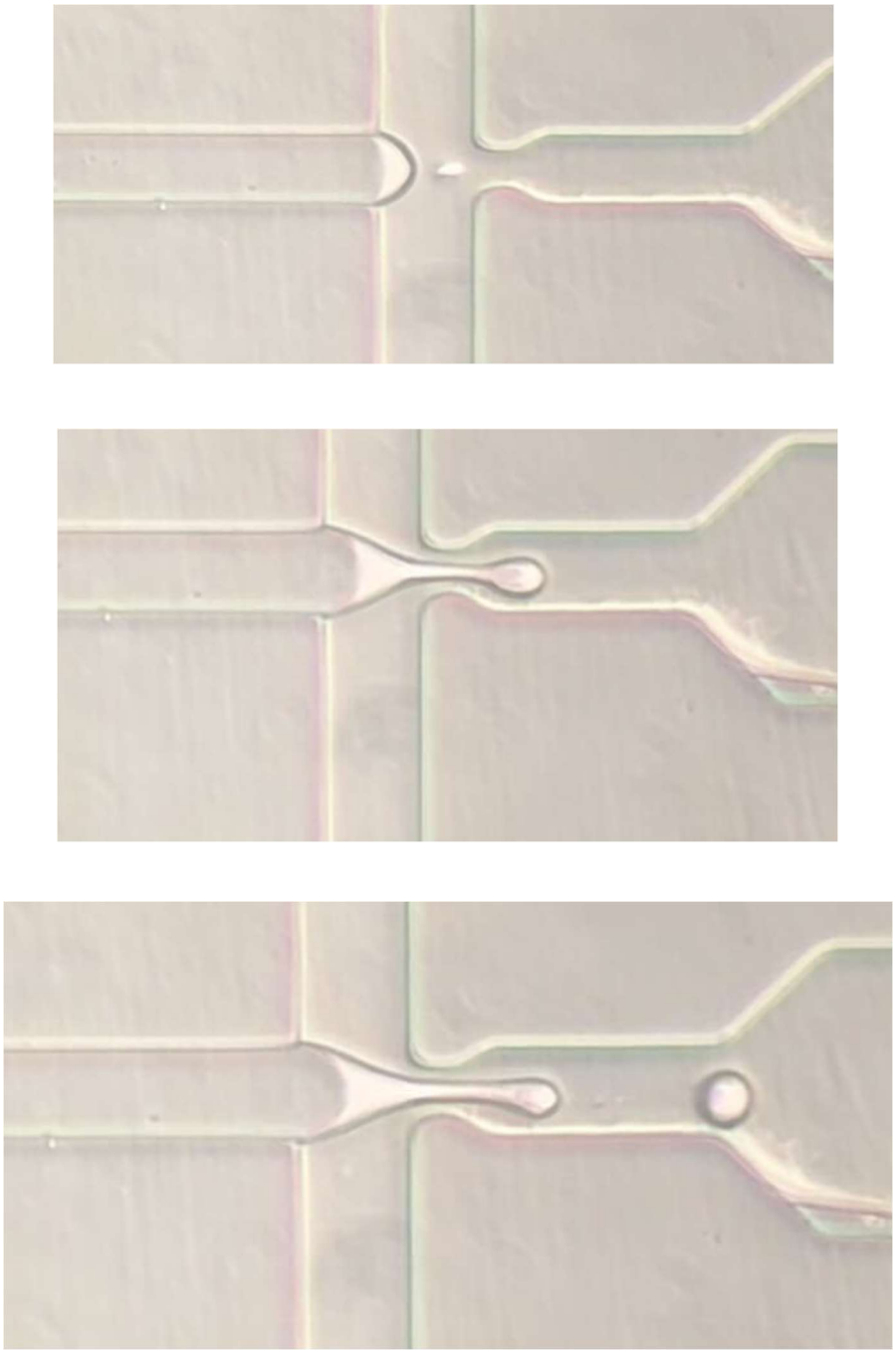

Figures 17-19: Droplet formation within microfluidic device using light microscopy (20X).

After collection, microbeads were morphologically and mechanically characterized using ImageJ and AFM, respectively. Using a sample of 500 beads, a combination of thresholding and analyze particles functionality revealed an average bead diameter 7µm with a standard deviation of 3µm. 25µL of the $CaCl_2$ solution containing the microbeads was pipetted onto an AFM dish and allowed to dry at 60℃ for 15 minutes and was subsequently transported to the Huson Laboratory for mechanical characterization. AFM revealed a Young's modulus of 2.6kPa, which is within the range of accepted values for alginate microbead stiffness based on existing literature.

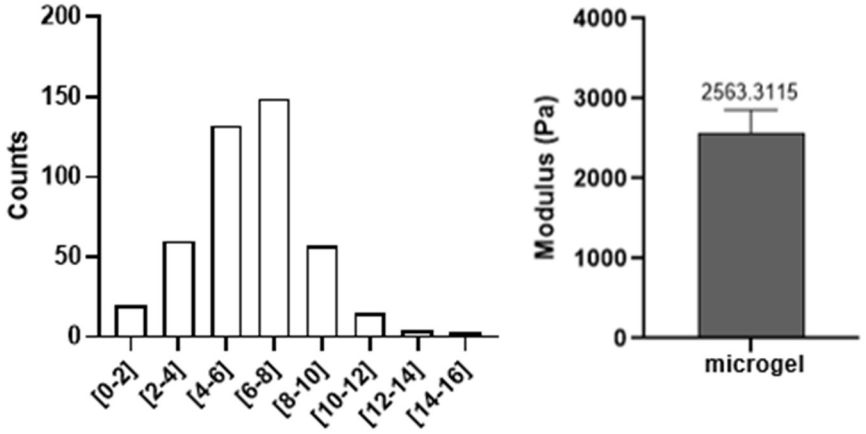

Figure 20: Histogram representing size distribution of collected alginate microbeads (n = 500, d in µm)

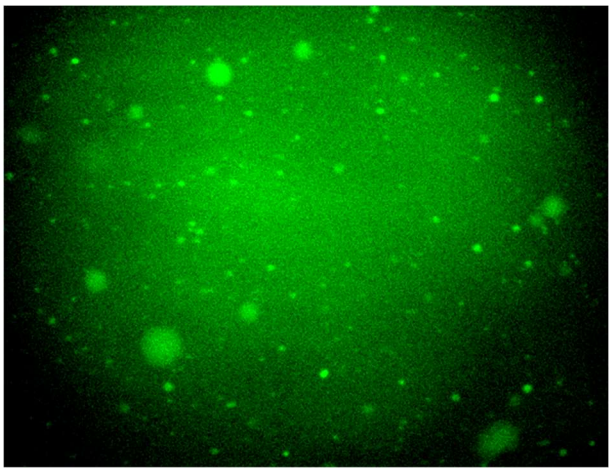

Figure 21: Fluorescence microscopy was used to visualize microbeads in solution.

Tumorsphere Encapsulation of Microbeads

To encourage microbead encapsulation by glioblastoma stem cells (GSCs), a hanging drop method was employed. This simple technique facilitates tumorigenesis and the uptake of microbeads by leveraging gravitational forces. A mixture of microbeads and GSCs are pipetted onto the lid of a 6-well, tissue-culture treated plate and inverted over a 1X PBS solution. The inversion results in a migration of cells and microbeads toward the bottom of the droplet & the PBS below evaporates over time, keeping the solution hydrated. Full encapsulation of deformable microgels paired with spheroid development over time allows for calculation of compressive stress.

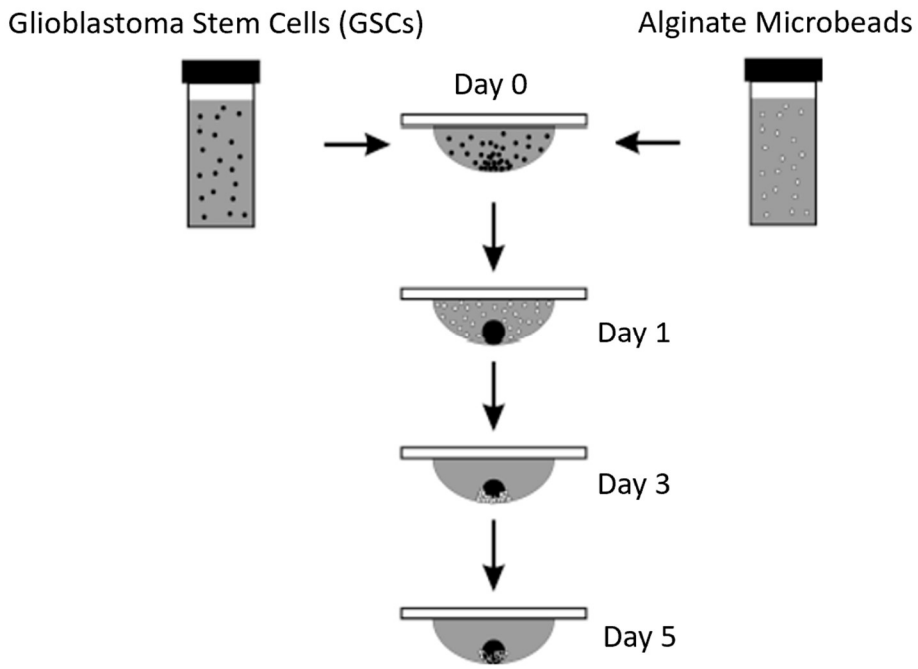

Figure 22: Schematic representation of the hanging drop method for tumorigenesis and microbead encapsulation. Microscopy performed on Days 1, 3, and 5 to evaluate spheroid progression.

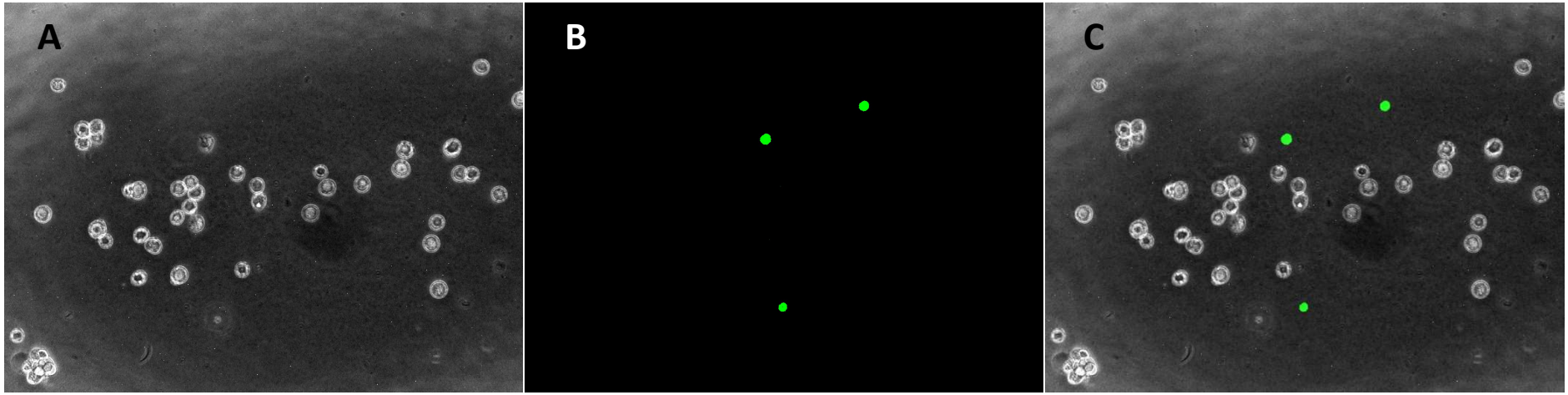

Figure 23: Day 1 of hanging drop; Brightfield view of GSCs and microbeads (A), Fluorescent view of microbeads (FITC) (B), and merge of images A and B (C).

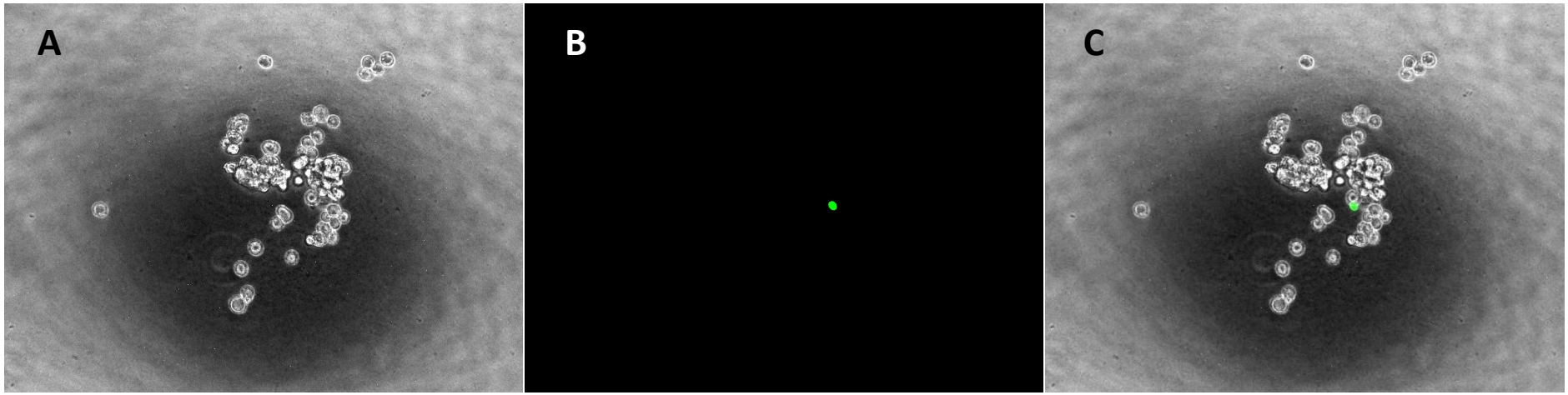

Figure 24: Day 3 of hanging drop; Brightfield view of GSCs and microbead (A), Fluorescent view of microbead (FITC) (B), and merge of images A and B (C).

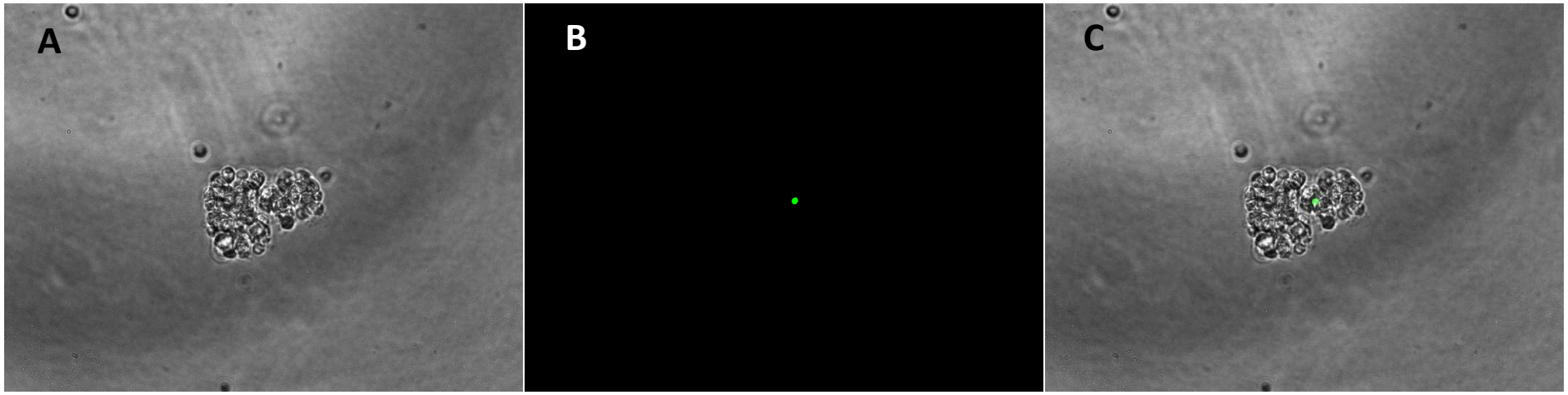

Figure 25: Day 5 of hanging drop; Brightfield view of GSCs and microbead (A), Fluorescent view of microbead (FITC) (B), and merge of images A and B (C).

As demonstrated by Figure 22 (schematic), the hanging drop results in a gradual migration and coalescence of GSCs and microbeads as gravitational forces act on the particles for five days. Figure 23 shows beads scattered about cells with no discernable pattern or direction. Figure 24 shows movement of both GSCs and a sole microbead toward the center of the image, which represents the focus of the droplet. Lastly, Figure 25 shows full encapsulation of the microbead by the newly formed spheroid. It should be noted that the hydrogels in Figure 23 are not in the exact focal plane as the GSCs due to the 3D nature of this experimental design. However, this is corrected in Figures 24 and 25 as all particles in question occupy neighboring space.

Finite Element Analysis

Finite element analysis (FEA) is the use of calculations, models, and simulations to predict and understand how an object might behave under prescribed physical conditions. For instance, a civil engineer might conduct FEA to determine the conditions (i.e., load) under which a bridge may experience failure. A mechanical engineer may subject a 3D model or object to repetitive loading to assess vulnerabilities to fatigue. Similarly, bioengineers can leverage FEA to investigate how stress and strain impact human physiology. A 3D reconstruction of a femoral head and neck within a hip joint may be repeatedly loaded to simulate walking and provide insight into structural deficits likely to result in injury over time. For the purposes of this thesis, FEA will be used to approximate total elastic compression of encapsulated alginate microbeads which, paired with the elastic modulus, allows for calculation of spheroid force generation.

We used the general case of two deformable spheres in contact to approximate the interaction between GSCs and microbeads, which is depicted in the schematic below and is described by the equations that follow. It should be noted that this model assumes that the two spheroid in contact do *not* possess the same elastic modulus (i.e., they are not comprised of the same material). Further, the two spheres depicted exhibit a significant difference in diameter, which results in varying degrees of elastic compression. The purpose of size constraint for microbead synthesis (via well-defined microfluidic channels) was approximation of cell diameter. In other words, one microbead at the center of a tumorsphere represents what a single-cell may experience as a result of tumor evolution.

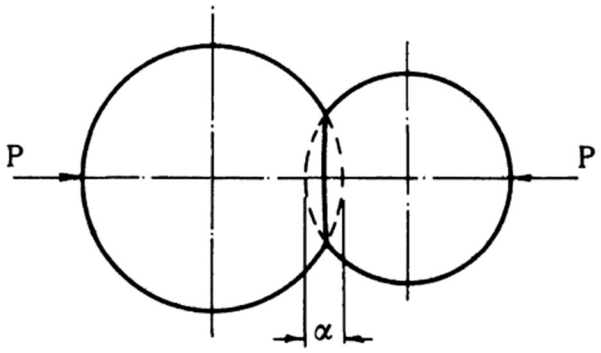

Figure 26: Schematic of two deformable spheres in contact, where P represents total applied force and α represents total elastic compression (Puttock, NSLT No. 25)

$$\alpha = \frac{(3\pi)^{\frac{2}{3}}}{2} * P^{\frac{2}{3}} * (V_1 + V_2)^{\frac{2}{3}} * \left(\frac{1}{D_1} + \frac{1}{D_2}\right)^{\frac{1}{3}} \quad (3)$$

and

$$V = \frac{(1 - \sigma^2)}{\pi * E} \quad (4)$$

where: α = total elastic compression

P = total applied force

D = diameter of sphere

σ = Poisson's ratio

E = elastic modulus

Alginate microbeads will be in direct contact with *many* cells rather than a single cell along a well-defined axis. Thus, the model and equation (3) have been adjusted accordingly. In the following diagram, the green center represents the microbead at the "core" of a growing tumorsphere with cells collected around. It can be assumed that each of the cells comprising any given spheroid are approximately the same size and are

therefore capable of generating similar amounts of force, represented by the variable *P*. The green dotted line represents the perimeter of an ideal, uncompressed bead.

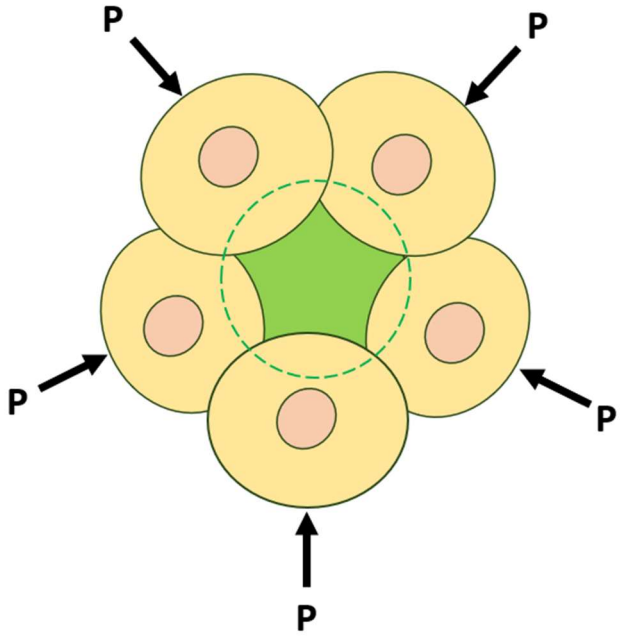

Figure 27: Alginate microbead subjected to compressive stress resulting from spheroid encapsulation.

$$\alpha = \frac{(3\pi)^{\frac{2}{3}}}{2} * (P_1 + \cdots + P_n)^{\frac{2}{3}} * (V_1 + \cdots + V_n)^{\frac{2}{3}} * \left(\frac{1}{D_1} + \cdots + \frac{1}{D_n}\right)^{\frac{1}{3}} \quad (5)$$

where: α = total elastic compression

P = total applied force

D = diameter of sphere

σ = Poisson's ratio

E = elastic modulus

n = number of GSCs in direct contact with microbead(s) resulting in elastic deformation.

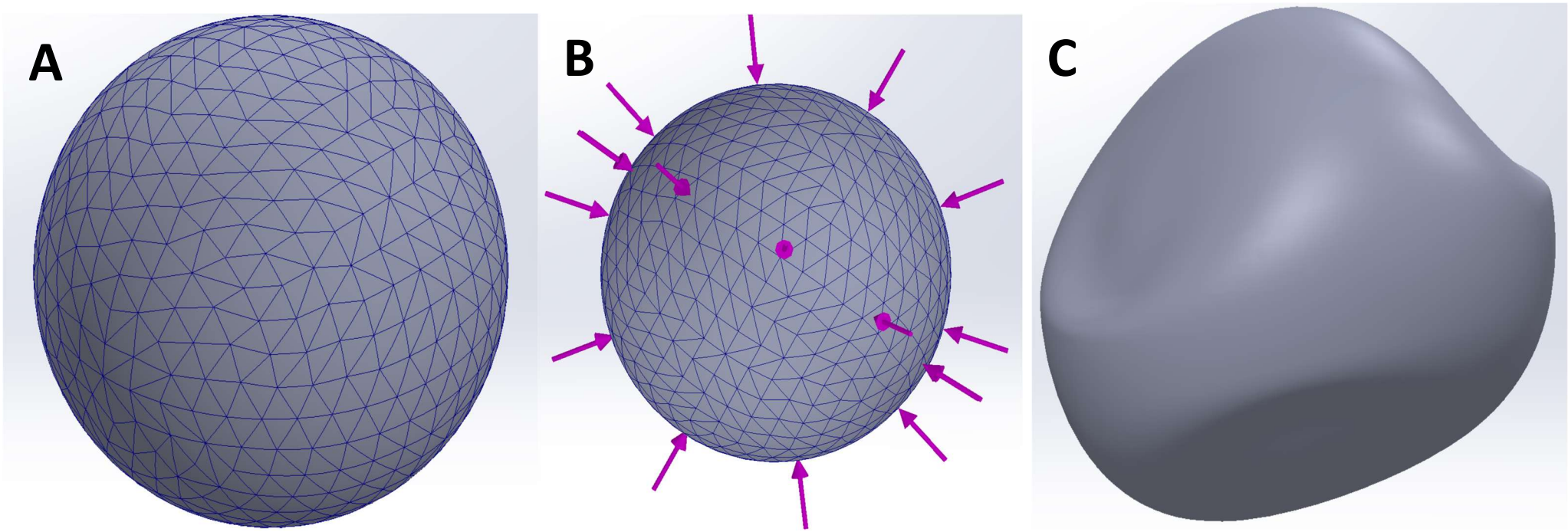

Figure 28: Generation of a sphere by revolving circular sketch around central axis and discretization(A); Application of circumferential external forces to discretized sphere (B); Resulting 3D deformation profile.

SOLIDWORKS 3D modeling software, in combination with fluorescent and confocal microscopy, can be used to accurately reconstruct the deformation experienced by each microbead. This involves generation and discretization of a sphere, which is a process by which the continuous surface is transferred into discrete, defined counterparts. Using the following method, we are able to produce a 3D deformation profile by extracting 2D morphological changes.

IV. CONCLUSIONS

In conclusion, we have demonstrated ultrastructural, mechanical, and compositional changes within the TME associated with tumor evolution and disease progression. Here, using a combination of biological and bioengineering tools, such as AFM, SEM, and IF microscopy, we found that tumor core is stiffer, less porous, and exhibits elevated concentrations of key ECM proteins when compared to both tumor rim and to healthy controls. Further, we have contributed to a growing body of literature exploring tumor heterogeneity as a key biophysical driver of glioblastoma development. This provides context for the aberrant interactions between the TME and the tumor itself and marks the distinction between inter- and intra-tumor aspects of disease progression.

We continued to build a bioengineering platform for the development of monodisperse, fluorescent, homogenous, deformable alginate microbead that act as a force probe to investigate the relationship between tumor development and intra-tumoral compressive stress. Using a microfluidic device design that incorporated a flow-focusing junction, spherical alginate hydrogels we synthesized, collected, and mechanically and morphologically characterized. Principles of fluid dynamics such as dynamic viscosity, interfacial tension, and capillary number informed specific parameters of fluid flow to optimize alginate bead production. A hanging drop method was employed to encourage the uptake of microbeads by glioblastoma stem cells, which readily form spheroids and pseudo-tumors under cell culture conditions. We successfully embedded fluorescent alginate microbeads into growing tumorspheres and utilized time-lapse microscopy,

fluorescence microscopy, and confocal microscopy to evaluate encapsulation progress and therefore demonstrated successful tool development.

Next, finite element analysis was used to model the deformation experienced by microbeads subjected to compressive stress generated by GSC tumorspheres. Discretization of an ideal sphere and subsequent application of external load resulted in a deformation profile that can be used to calculate elastic compression. Here, we can extrapolate compressive information and supplement the governing equations of elastic to calculate total applied force. In all, we have developed a force probe capable of quantifying intra-tumoral compressive stress generated in glioblastoma development.

Future work utilizing this bioengineering platform might involve the generation of *larger* alginate microbeads, perhaps on the order of 100-150μm in diameter to act as a pseudo-core, as this would allow tumorspheres to grow much larger and enhance the longitudinal aspect of our studies. Our laboratory is equipped to fabricate biomimetic platforms for 3D cell culture. This allows us to modulate external stimuli, such a ECM stiffness and composition, and could be used in tandem with this force probe to investigate biophysical responses to extrinsic alterations. Additionally, this tool could be used to evaluate stress and strain relationships in other tissues, such as cardiac remodeling.

REFERENCES

[1] Dubrow, Robert, and Amy S. Darefsky. "Demographic Variation in Incidence of Adult Glioma by Subtype, United States, 1992-2007." *BMC Cancer* 11.1 (2011): 325. Print.

[2] Krex, Dietmar, et al. "Long-Term Survival with Glioblastoma Multiforme." *Brain* 130.10 (2007): 2596-606. Print.

[3] Dolecek, Therese A., et al. "CBTRUS Statistical Report: Primary Brain and Central Nervous System Tumors Diagnosed in the United States in 2005–2009." *Neuro-Oncology* 14.suppl_5 (2012): v1-v49. Print.

[4] Hoelzinger, Dominique B., et al. "Gene Expression Profile of Glioblastoma Multiforme Invasive Phenotype Points to New Therapeutic Targets." *Neoplasia* 7.1 (2005): 7-16. Print.

[5] Alfardus, Huda, et al. "Intratumour Heterogeneity in MicroRNAs Expression Regulates Glioblastoma Metabolism." *Scientific Reports* 11.1 (2021): 15908. Print.

[6] Rasband, Matthew N. “Glial Contributions to Neural Function and Disease.” *Molecular & Cellular Proteomics : MCP* vol. 15,2 (2016): 355-61.

[7] Wolf, Kayla J et al. “Dissecting and rebuilding the glioblastoma microenvironment with engineered materials.” *Nature Rev. Materials* vol. 4,10 (2019): 651-668.

[8] Dhamecha, Dinesh et al. “Applications of alginate microspheres in therapeutics delivery and cell culture: Past, present and future.” *International Journal of Pharmaceutics* vol. 569 (2019): 118627

[9] Chen, Wanyu et al. “Microfluidic one-step synthesis of alginate microspheres immobilized with antibodies.” *Journal of the Royal Society, Interface* vol. 10,88 20130566. 21 Aug. 2013

[10] Utech, Stefanie et al. “Microfluidic Generation of Monodisperse, Structurally Homogeneous Alginate Microgels for Cell Encapsulation and 3D Cell Culture.” *Advanced Healthcare Materials* vol. 4,11 (2015): 1628-33

[11] Micro/Nano Technology Center, University of Louisville. *Creating PDMS Molds with SU8 SOP.* Oct. 2013.

[12] Garstecki, Piotr, et al. "Formation of Droplets and Bubbles in a Microfluidic T-Junction—Scaling and Mechanism of Break-Up." *Lab on a Chip* 6.3 (2006): 437-46. Print.

[13] Moiseeva, E. V., A. A. Fletcher, and C. K. Harnett. “Thin-Film Electrode Based Droplet Detection for Microfluidic Systems.” *Sensors and Actuators B: Chemical* 155 (1): 408–414. 2011

[14] Puttock, M.J. and Thwaite, E.G.”Elastic Compression of Spheres and Cylinders at Point and Line Contact.” *National Standards Laboratory Technical Paper No. 25*. Commonwealth Scientific and Industrial Research Organization, Australia 1969.

CURRICULUM VITA

Education

Bachelor of Science (B.S.) in Bioengineering — Awarded August 2022
Master of Engineering (M.Eng.) in Bioengineering — Awarded August 2023

Manuscripts in Review or Preparation

Zachary P Fowler*, Bradley J Mahaffey*, Zoe Lung, Vivien Dang, Joseph Chen**, "**ECM Composition and Organization Underlie Mechanical Signatures of Glioblastoma Core and Rim**"** *Sci Reports***.**

Peer-Reviewed Abstract Presentations

Eric Dong*, **Zachary P. Fowler**, and Joseph Chen, "Optimizing Decellularization Strategies for Glioblastoma Core and Rim Tissue", Research! Louisville, Louisville, KY, Sep. 21, 2022

Zachary P. Fowler*, Bradley J. Mahaffey*, and Joseph Chen, "Glioblastoma Core and Rim Exhibit Distinct Mechanical and Ultrastructural Signatures", BMES 2022, San Antonio, TX, Oct. 12-15, 2022.

Bradley J Mahaffey*, **Zachary P Fowler***, Zoe Lung, Vivien Dang, Neha Anil, Marco Munoz, Joseph Chen, "Quantification of Tumor Biophysical Heterogeneity Through Mechanical and Ultrastructural Analysis", Summer Bioengineering Conference, Vail, CO, June 5-9, 2023

Zachary P. Fowler*, Cindy K. Harnett, Joseph Chen, "Microfluidic Generation of Alginate Beads to Quantify Intra-Tumoral Compressive Stress", NNCI Nano, Louisville, KY, July 25, 2023

Zachary P. Fowler*, McKenzie Johnson, Joseph Chen, "Quantification of Intra-Tumoral Compressive Stress in Glioblastoma Development", Brown Cancer Center Retreat, Louisville, KY, Sept. 15, 2023

Zachary P. Fowler*, McKenzie Johnson, Joseph Chen, "Alginate Hydrogel Probe for Quantifying Intra-Tumoral Compressive Stress", BMES, Seattle, WA, Oct. 11-14, 2023